



Research Article

## The optimal geometric design of a v-corrugated absorber solar air heater integrated with twisted tape inserts

Issam Ali ALJUBURY<sup>\*1</sup>, Mohammed KHALIL HUSSAIN<sup>2</sup>, Ammar FARHAN<sup>2</sup>

<sup>1</sup>Department of Mechanical Engineering, University of Baghdad, Iraq

<sup>2</sup>Department of Energy Engineering, University of Baghdad, Iraq

### ARTICLE INFO

#### Article history

Received: 03 September 2021

Accepted: 25 February 2022

#### Keywords:

Solar Air Heater;  
Multi-Objective Function;  
Efficiency; Optimization  
Algorithm

### ABSTRACT

The proper design of a solar air heater depends on the highest thermal performance of the solar collector. In the present paper, proposed a method to find an optimal dimension of V-corrugated absorber solar air heater (VSAH) combined with a twisted tape insert (TTI). The design variables of the VSAH-TTI are length, width, number of channels, and twisted tape ratio. The effect of each design variable is examined and studied under various ranges of Reynolds number (Re). Given the complexity in changing design variables of solar collector having a V-corrugated absorbing plate with twisted tape insert (VSAH-TTI) to find the highest thermal performances, the multi-objective function genetic algorithm is used to find the optimal dimensions of VSAH-TTI based on maximizing the heat gain, thermal and effective efficiency as well as minimizing the pressure drop on solar collector. The range of each design variable of the VSAH-TTI by means of length (1 – 2.5 m), width (0.5 – 1.5 m), number of channels (4 – 14), and twisted tape ratio (1 – 8) are specified in paper based on the most common practical values of the solar collector. The results showed for the case under study that each design variable of VSAH-TTI affect the thermal performance and the optimized geometry by using a genetic algorithm (Ga) can find the optimal geometric dimensions of VSAH-TTI. The optimal dimension by using Ga can increase the heat gain by more than 8% and increase the effective and thermal efficiency of more than 7% for the original geometry. Furthermore, the optimized geometry can reduce more than 29% for the original geometry. These improvements in optimized geometry for VSAH-TTI without introducing any additional items.

**Cite this article as:** Aljubury I A, Khalil Hussain M, Farhan A. The optimal geometric design of a v-corrugated absorber solar air heater integrated with twisted tape inserts. J Ther Eng 2023;9(2):478–496.

#### \*Corresponding author.

\*E-mail address: [drissam@uobaghdad.edu.iq](mailto:drissam@uobaghdad.edu.iq), [mohammedkhalil@uobaghdad.edu.iq](mailto:mohammedkhalil@uobaghdad.edu.iq), [ammarali@uobaghdad.edu.iq](mailto:ammarali@uobaghdad.edu.iq)

*This paper was recommended for publication in revised form by Regional Editor Baha Zafer*



## INTRODUCTION

Solar air heaters (SAH) are considered one of the most practical engineering systems employed for harvesting solar radiations and converting them into useful heat energy used for heating purposes that works based on renewable power. SAHs are widely used for residential heating and crop drying devices, water heating, solar desalination, paint spraying operations as well as a wide range of engineering applications [1]–[6]. In the solar air heaters system, heat is transferred from the absorber plate to the air which passes over this plate by natural or forced convective heat transfer. Since all types of solar air collectors have two inherent disadvantages i.e., low heat capacity and poor thermal conductivity, which leads to a small amount of convective heat transfer inside the airflow channel in the solar air collector [7]. Laminar boundary sub-layer is formed in the case of using smooth flat plate in the solar air collector over the surface of the absorber plate, which leads to the low thermal performance of the collector, therefore, to achieve high efficiency, it is necessary to add roughness on the underside surface of the absorber plate or creating extended surfaces (fins) to breakdown these laminar sub-layers [8], [9].

Considerable efforts and various experimental and theoretical research methodologies have been done to maximize this rate of heat transfer from solar air collectors [10]. Many types of design ideas are suggested and utilized to enhance and maximize the coefficient of heat transfer between the air and surface of the absorber plate of the SAH. These suggestions showed a good enhancement in the thermal-hydraulic performance as a result of utilizing the different geometrical design of artificial surface roughness placed on the underside surface of the absorber plate collector, such as various and multiple V-shaped ribs [11], [12], Wedge ribs [13], transverse ribs [14], wavy wire mesh [15], wavy grooved ribs [16], inclined ribs [12], chamfered ribs [17], wavy arc ribs [18], etc. The artificial roughness over the absorber plate can be fabricated or created machining. The ribs utilized in solar air collectors have various cross-section areas such as circular, semi-circular, elliptical, triangular square, rectangular, dimple protrusions, chamfered [19], etc. Besides, the heat transfer and airflow dynamics over the absorber plate of the solar collector depend greatly on the shape and orientation of the ribs. Therefore, research studies on enhancing the thermo-hydraulic performance analysis of the solar air collectors are critical in engineering applications [20]. In the previous literature, several techniques applied for the optimization of solar air heaters have been used.

Gupta and Kaushik [21] studied the energy and exergy performance of a flat-plate solar air heater to determine the optimum design parameters. Results revealed that there is an optimal inlet air temperature correlated with the optimal mass of airflow rate per unit area of the absorber plate for any value of aspect ratio and the depth of the duct. Nwosu

[22] used the exergy optimization technique to optimize the design configuration of cylindrical fins over an absorber plate of the solar air heater with absorptive coating. Results explained that the performance of the optimized cylindrical fins enhances the rate of absorption and dissipation heat of the solar air collector. Thermo hydraulic optimization of the solar air collector with artificial roughness of chamfered repeated ribs with grooves in between on the absorber plate presented by Layek [23]. Results revealed that there is exists a set of optimal values of roughness parameters that yield maximum effective efficiency for the solar air collector according to the specified set of working conditions. Siddhartha et al. [24] developed and implemented a trained particle swarm optimization technique for exploring the maximum efficiency of solar air heater with smooth flat absorber plate using several operating variables. They studied a domain of optimizing parameters. Obtained results showed that the maximum thermal efficiency of solar air heater was 72.42%. Sahin [25] applied the genetic algorithm technique and artificial bee colony algorithm by determining the optimal operating parameters. Results revealed that the maximum thermal performance of the solar air heater was about 0.7998 with an optimized value of operation conditions and design variables. Kumar and Kim [26] presented a numerical optimization of solar air collectors having various kinds of artificial roughness shapes and sizes on the absorber plate to enhance the thermohydraulic and effective efficiencies of the ribbed collector. Results indicated that discrete multiple V-shaped ribs have high thermal and effective efficiency values compared with other types of the same roughness shapes and sizes. Prasad et al. [27] presented an optimization and analysis of the thermo-hydraulic performance of artificially roughened solar air heater to obtain maximum heat transfer. Results showed that the optimal thermo-hydraulic performance of three sides artificially roughened depends on the optimal value of roughness Reynolds number. Kulkarni et al. [28] carried out a study to predict the optimum design for improving the thermo-hydraulic performance of solar air collectors using a hybrid multi-objective genetic algorithm with coupling surrogate approximations. Results of the current optimization study explained that the design operating parameters have a considerable effect on the heat transfer rate and pressure losses. The teaching-learning-based optimization technique was developed by Rao and Waghmare [29] to get the optimal set value of design and operating variables to increase the thermal efficiency of solar air collectors. The obtained results indicated that the maximum thermal efficiency of the collector was about 76.67%. Zhuang et al. [30] carried out experimental research and developed a mathematical simulation model for heat transfer by solar air heater to predict thermal efficiency and effective efficiency by optimizing the structure of a solar collector. Results revealed that maximum thermal efficiency of collector achieved using minimum perforation spacing, plate

spacing, and thickness of air layer, while the higher pressure drops within the collector due to friction resistance.

An experimental and theoretical parametric optimization research was conducted by Acir et al. [31] to set the optimal operating parameters affecting energy and exergy efficiencies of the solar air collector. The obtained results revealed the maximum computed energy efficiency (68.1%) and exergy efficiency (34.4%) using the optimum parameters. An experimental and optimization study was performed by Nadda et al. [32] to investigate the heat transfer and friction characteristics and maximize the overall performance of the solar air collector using air impingement jets. The experimental results illustrated that using air impingement jets leads to an augment in the thermal efficiency of the solar collector. Ansari and Bazargan [33] studied experimentally the effect of repeated ribs on the absorber plate of the solar air collectors to improve the thermal efficiency. The genetic algorithm was used to obtain the optimum values of each one of the design parameters for ribs configuration. They illustrated that utilizing ribs increases the thermal efficiency of the solar air heater by about 9%.

The thermo-hydraulic performance of solar air heater with a flat absorber plate of three arcs rib roughness was evaluated and optimized by Kumar et al. [34]. Results showed that there was a good enhancement in thermal efficiency of solar air collectors when changing roughness parameters meanwhile pumping electrical power increased and leads to an increase in pressure losses. Yildirim and Özdil [35] theoretically investigated thermal

and thermohydraulic efficiencies of solar air heater having various geometrical roughness parameters (ribs and grooves) attached to the absorber plate then compared the results with the flat plate solar air collectors. Results showed that both thermal efficiency and thermohydraulic of the collector with ribs and grooves absorber has superiority on smooth absorber plate and increase by increasing Reynolds number ( $Re$ ) for all roughness parameters. Qader et al. [36] performed a study on CFD to investigate the effect of fins inclination on the thermal and hydraulic efficiency of the solar air collector using response surface methodology. The study mainly focused on analyzing and quantifying the influence of changing various parameters to determine the optimum value of these parameters to achieve maximum thermal-hydraulic performance.

A numerical simulation using CFD code based on the optimization method was carried out by Bezbaruah et al. [37]. Optimization results according to the design geometric parameters demonstrated an enhancement in the ratio of Nusselt number and friction factor.

From the previous literature review, many scientific researchers are still investigating techniques to enhance the thermal-hydraulic performance of SAHs. A multi-objective function optimization algorithm will be used to investigate different design variables of the VSAH- TTI such as length and width of collector, number of channels, and twisted tape ratio to maximize thermal and effective efficiency as well as minimize the pressure drop on the solar collector. However, few studies have focused on the combination of

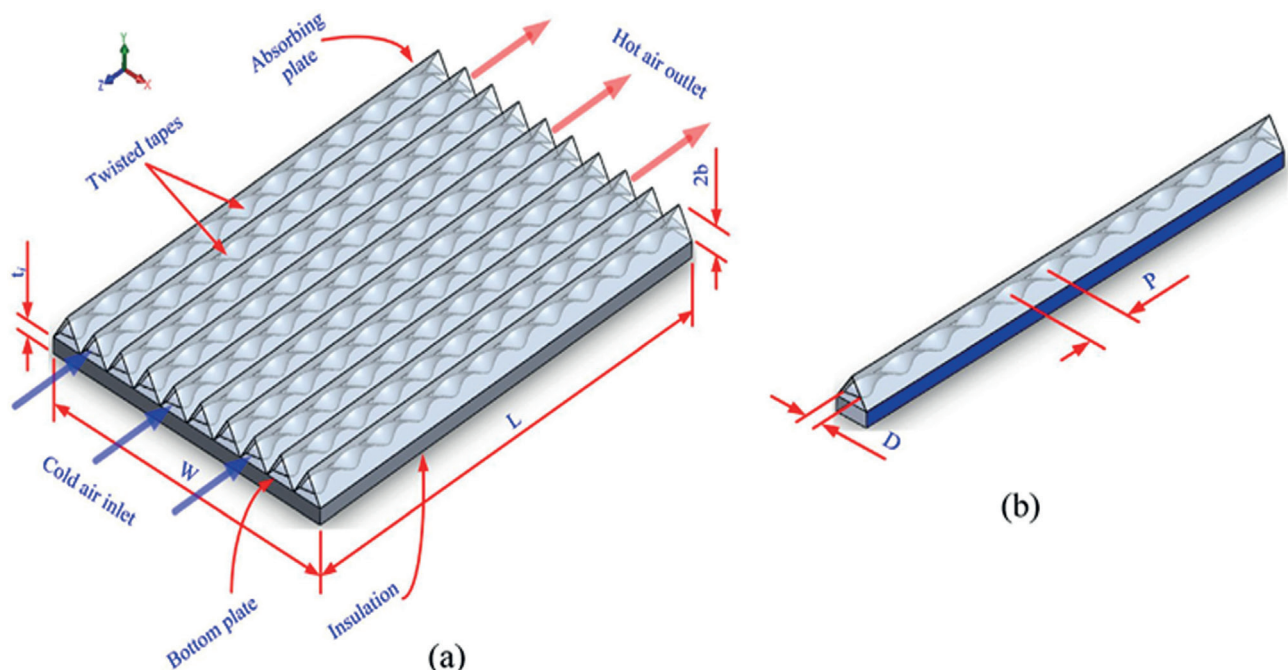


**Figure 1.** Schematic view of (a) VSAH, and (b) triangular airflow channel [38].

a V-corrugated absorber solar air heater (VSAH) with a twisted tape insert (TTI). Therefore, a mathematical model of VSAH-TTI will be developed based on the energy balance technique by using a genetic algorithm to find the optimal dimensions of VSAH-TTI.

The present study proposed a procedure to find the optimal dimensions of the VSAH- TTI by using a multi-objective function optimization algorithm. The design variables of the VSAH- TTI are the length of the collector, the width of the collector, the number of channels, and the twisted tape ratio. Each design variable has specific constraints based on the most common practical values. To find the optimal geometric dimensions, the main objectives in the multi objectives genetic algorithm to be maximized are the heat gain, thermal and effective efficiency as well as to be minimized the pressure drop on the VSAH- TTI.

### NUMERICAL ANALYSIS

Poor convective heat transfer coefficient between absorbing plate and airflow results in low thermal performance and high thermal losses. Therefore, using a V-corrugated absorber plate leads to an increase in the convective heat transfer area which enhances the thermal efficiency of the solar collector. Furthermore, the integration of VSAH with TTI is envisaged to have the best thermal performance than that of VSAH without TTI. Two VSAHs with and without TTI are investigated in the present work as presented in Fig. 1.

Each VSAH consists of a single transparent cover, a V-corrugated absorbing plate, a bottom plate, and Holz100 Thermal walls used for back insulation. A triangular flow channel was formed by the absorbing and bottom plates where the airflow carried the energy from the heated surface.

### ENERGY BALANCE EQUATIONS

Energy flow between the VSAH elements is depicted in Fig. 2. To simplify the mathematical model without obscuring the basic physics law, assumptions are taken to derive the energy balance equations for each element of the VSAH as follows [39].

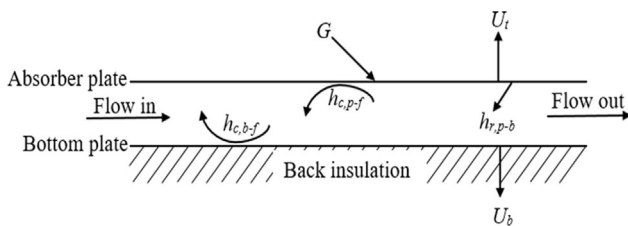


Figure 2. Energy flow diagram between elements of VSAH.

- (i) Quasi-steady-state conditions are used to model the elements of VSAH.
- (ii) The one-dimensional flow of heat between VSAH components.
- (iii) Neglect the side losses.
- (iv) Sky temperature is used to compute the thermal radiation between VSAH elements and the environment.

Based on the energy flow diagram between VSAH components, the energy equilibrium equation for heated surface, airflow, and bottom plate are written below, respectively.

$$\tau_c \alpha_p G = U_t(T_p - T_{amb}) + h_{r,p-b}(T_p - T_b) + h_{p-f}(T_p - T_f) \quad (1)$$

$$\frac{2\dot{m}_c}{A_p}(T_f - T_{fi}) = h_{p-f}(T_p - T_f) + h_{b-f}(T_b - T_f) \quad (2)$$

$$h_{r,p-b}(T_p - T_b) = h_{b-f}(T_b - T_f) + U_b(T_b - T_{amb}) \quad (3)$$

where  $T_p$ ,  $T_b$ ,  $T_f$  and  $T_{amb}$  are the temperature of the absorbing plate, bottom plate, airflow, and ambient, respectively.  $h_{p-f}$  and  $h_{b-f}$  are convective heat transfer coefficients between heated surface and airflow, and between the bottom plate and airflow, respectively.  $h_{r,p-b}$  is the radiative heat transfer coefficient between absorbing and bottom plates.  $U_t$  and  $U_b$  are the coefficient of top and bottom heat loss, respectively.  $G$  is the incoming solar radiation.

Eqs. (1-3) are solved simultaneously to compute the temperature of each VSAH component. Thus, the linked coefficients of heat transfer are evaluated firstly from the following relations.

Duffie and Beckman [39] suggested the below equation to evaluate the top coefficient of heat losses with an error percentage of  $\pm 0.3 \text{ W/m}^2\text{K}$ .

Duffie and Beckman [39] suggested the below equation to evaluate the top coefficient of heat losses with an error percentage of  $\pm 0.3 \text{ W/m}^2\text{K}$ .

$$U_t = \left[ \frac{N_c}{\frac{C}{T_{mp}} \left( \frac{T_{mp} - T_{amb}}{N_c + F} \right)^e + \frac{1}{h_w}} \right]^{-1} \quad (4)$$

$$+ \frac{\sigma(T_{mp} - T_{amb})(T_{mp}^2 - T_{amb}^2)}{1 + \frac{2N_c + F - 1 + 0.133\epsilon_p}{\epsilon_p} - N_c}$$

$$F = (1 + 0.089h_w - 0.1166h_w\epsilon_p)(1 + 0.07866N_c) \quad (5)$$

$$C = 520(1 - 0.000051\beta^2) \text{ for } 0^\circ < \beta < 70^\circ \quad (6)$$

$$e = 0.43 \left( 1 - \frac{100}{T_{mp}} \right) \quad (7)$$

$$h_w = 5.7 + 3.8 V_w \quad (8)$$

where  $N_c$  is the cover numbers,  $b$  is the collector inclined angle of the collector,  $h_w$  is the wind heat transfer coefficient,  $\sigma$  is the Stefan–Boltzmann constant.  $\epsilon_p$  and  $\epsilon_c$  are the emittance of heated surface and cover, respectively.

The bottom heat loss between the bottom plate and the environment is found as follows.

$$U_b = \frac{\lambda_i}{\delta_i} \quad (9)$$

where the  $\lambda_i$  and  $\delta_i$  are the thermal conductivity and thickness of insulation, respectively.

The radiation heat transfer coefficient between the absorber and the bottom plates is given by.

$$h_{r,p-b} = \frac{\sigma(T_p^2 + T_b^2)(T_p + T_b)}{\frac{1}{\epsilon_p} + \frac{1}{\epsilon_b} - 1} \quad (10)$$

For smooth VSAH, Nusselt number ( $Nu_s$ ) related to convective heat transfer coefficient between absorber plate and the airstream is given by following equation [40].

$$Nu_s = Nu_o + \alpha_o \frac{b}{L} n \quad (11)$$

where  $Nu_o$  and  $\alpha_o$  are functions of Reynolds number ( $Re$ ),  $L$  is the collector length, and  $n$  is the number of collectors linked in a series.

$$Nu_o = 2.821 \text{ and } \alpha_o = 0.126Re \text{ for } Re < 2800 \quad (12a)$$

$$Nu_o = 1.9 \times 10^{-6} Re \text{ and } \alpha_o = 225 \text{ for } 2800 \leq Re \leq 10^4 \quad (12b)$$

$$Nu_o = 0.0302Re^{0.74} \text{ and } \alpha_o = 0.242 Re^{0.74} \text{ for } 10^4 < Re < 10^5 \quad (12c)$$

$$Re = \frac{4\rho V_{in} b}{3\mu} \quad (13)$$

where  $b$  is the half-height of the flow passage.

For VSAH with TTI, Hong and Bergles [41], and Bas and Ozceyhan [42] reported empirical relations of  $Nu$  for laminar and turbulent flow through a duct, respectively.

$$Nu = 5.172 \left( 1 + 5.484 \times 10^{-3} Pr^{0.7} \left( \frac{Re}{Y} \right)^{1.25} \right)^{0.5} \quad (14)$$

$$Nu = 0.6Re^{0.57} Y^{-0.45} Pr^{0.4} \quad (15)$$

$$Y = \frac{P}{D} \quad (16)$$

Convective heat transfer coefficients between airflow and absorbing and bottom plates are assumed to equal and compute as follows [38].

$$h_{p-f} = h_{b-f} = \frac{\lambda Nu}{D_h} \quad (17)$$

Thermo-physical properties are computed using the bulk mean air temperature ( $T_{fm}$ ) from the following empirical expressions [43].

$$\rho = \frac{101325}{287.045 \times T_{fm}} \quad (18a)$$

$$\lambda = 0.0257 \times \left( \frac{T_{am}}{293} \right)^{0.086} \quad (18b)$$

$$\mu = 1.81 \times 10^{-5} \times \left( \frac{T_{am}}{293} \right)^{0.735} \quad (18c)$$

$$c_p = 1006 \times \left( \frac{T_{am}}{293} \right)^{0.0155} \quad (18d)$$

## HYDRO-THERMAL AND THERMAL PERFORMANCE

Thermal efficiency ( $\eta_{th}$ ) of a SAH can be defined based on the first law of thermodynamics as the conversion of incoming solar radiation to useful energy gain ( $Q_u$ ) by airflow. Thus,  $\eta_{th}$  is computed by dividing the useful energy gained by airflow to the solar irradiance that falls on the collector area as follows.

$$\eta_{th} = \left( \frac{Q_u}{GA_p} \right) \quad (19)$$

$$Q_u = \dot{m}_p c_p (T_{fo} - T_{fi}) \quad (20)$$

where  $T_{fo}$  and  $T_{fi}$  are the outlet and inlet airflow temperatures, respectively.

The presence of TTI has increased the friction losses across the flow channel, which is found to increase of consuming pumping power required to drive air across the SAH. Thereby, it is necessary to select TTI parameters that produced minimum friction factor, whereas keeping the coefficient of heat transfer is augmented to the maximum value. Cortes and Piacentini [44] defined the hydro-thermal efficiency ( $\eta_{h-th}$ ) which is the ratio between net energy gain by the airflow to the insolation falls on the collector area which is given by.

$$\eta_{h-th} = \frac{Q_u - \frac{P_p}{C_f}}{GA_p} \quad (21)$$

Where  $C_f$  is the energy conversion factor and  $P_p$  is the pumping power consumption to force air across the duct, which is given by the following equation.

$$P_p = \frac{\dot{m}\Delta P}{\rho} \quad (22)$$

The pressure drop ( $\Delta P$ ) throughout the air duct could be calculated as follows [45].

$$\Delta P = \frac{2fL_1\dot{m}^2}{\rho A_c^2 D_h} \quad (23)$$

where friction factor ( $f$ ) for smooth VSAH is given by [46]

$$f = f_0 + \gamma \frac{b}{L} n \quad (24)$$

where  $f_0$  and  $\gamma$  are function of the  $Re$  as written below

$$f_0 = 13.33Re^{-1} \text{ and } \gamma = 0.65 \text{ for } Re < 2800 \quad (25a)$$

$$f_0 = 3.2 \times 10^{-4} Re^{0.34} \text{ and } \gamma = 2.94Re^{-0.19} \text{ for } 2800 \leq Re \leq 10^4 \quad (25b)$$

$$f_0 = 0.0733Re^{-0.25} \text{ and } \gamma = 0.51 \text{ for } 10^4 \leq Re \leq 10^5 \quad (25c)$$

For VSAH with TTI,  $f$  is predicted as follows [45].

$$f = 38.4 \left(\frac{Re}{Y}\right)^{-0.95} \text{ for } Re < 2800 \text{ and } \frac{Re}{Y} < 100 \quad (26a)$$

$$f = (8.8201 + 2.1193Y - 0.2108Y^2 - 0.0069Y^3) \left(\frac{Re}{Y}\right)^{-0.7} \text{ for } Re < 2800 \text{ and } \frac{Re}{Y} > 100 \quad (26b)$$

$$f = 12.32Re^{-0.45} Y^{-0.65} \text{ for } Re \geq 2800 \quad (26c)$$

### VALIDATION BY THE LITERATURE

A VSAH model without TTI and the MATLAB code are currently being verified mathematically. Comparisons are made between the current model's results for smooth VSAH and data from Ref. [47]. Inlet air temperature and insolation which are used in the present model for smooth VSAH are given in Table 1. Fig. 3 and Table 2 presented the variation of numerical values of absorbing plate and outlet air temperatures as a function of time against the experimental data of Ref. [47]. The values of MAE for the absorber plate and outlet air temperatures are 3.22%, and 3.15%, respectively. While the values of RMSE of the absorber plate and outlet air temperatures are 4.45%, and 3.42%, respectively. Therefore, reasonably good agreement between the two sets of values ensures the accuracy of the present model, which indicating that the proposed model is suitable for further investigation. The following equations are used to compute the MAE and RMSE values [48].

$$RMSE (\%) = 100 \times \sqrt{\frac{\sum_1^n \left(\frac{X_{sim,i} - X_{exp,i}}{X_{sim,i}}\right)^2}{n}} \quad (27)$$

$$MAE (\%) = \frac{100}{n} \sum_1^n \left| \frac{X_{sim,i} - X_{exp,i}}{X_{exp,i}} \right| \quad (28)$$

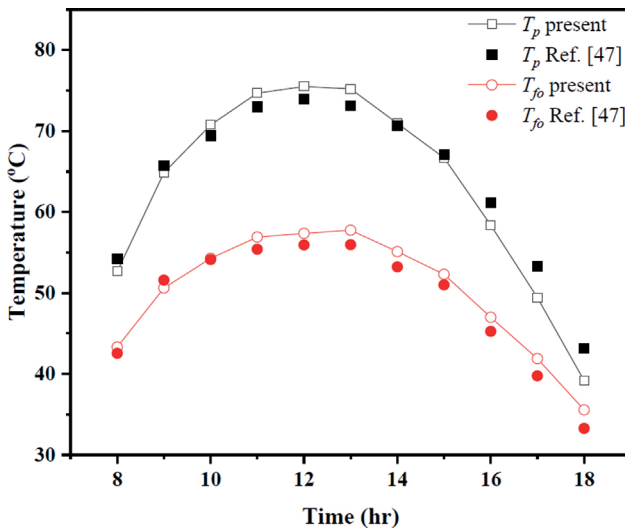


Figure 3. Comparison of the present study with experimental data of absorbing plate and outlet air temperatures given by Ref. [47].

### OPTIMAL GEOMETRIC DESIGN OF SOLAR AIR HEATER

Maximizing the heat gain, thermal and effective efficiency with minimizing the pressure drop is the main goal

Table 1. Inlet air temperature and solar irradiance data were used in the MATLAB code [47].

Time (hr)	$T_f$ (°C)	$G$ (W/m <sup>2</sup> )	Time (hr)	$T_f$ (°C)	$G$ (W/m <sup>2</sup> )	Time (hr)	$T_f$ (°C)	$G$ (W/m <sup>2</sup> )
8:00	33.9	460.7	12:00	38.0	966.3	16:00	35.3	573.0
9:00	35.7	734.1	13:00	39.1	928.8	17:00	34.3	367.0
10:00	36.9	865.2	14:00	38.4	831.5	18:00	32.0	168.5
11:00	38.0	943.8	15:00	37.2	745.3			

**Table 2.** Tabular values of Fig. 3.

Time (hr)	$T_p$ Ref. [43] (°C)	$T_p$ Present (°C)	$T_{fo}$ Ref. [43] (°C)	$T_{fo}$ Present (°C)
8:00	54.19	52.66	42.54	43.32
9:00	65.74	64.86	51.58	50.59
10:00	69.44	70.77	54.12	54.27
11:00	72.99	74.67	55.40	56.91
12:00	73.93	75.51	55.93	57.36
13:00	73.15	75.21	55.96	57.75
14:00	70.63	70.95	53.23	55.11
15:00	67.12	66.69	50.98	52.30
16:00	61.13	58.37	45.25	46.99
17:00	53.26	49.42	39.76	41.89
18:00	43.15	39.17	33.27	35.56

in the geometric design of solar air collectors. As shown in figure 1, the geometrical information of the solar collector with a twisted tape inserted are length, width, number of channels, and twisted tape ratio. The four main components in the design optimization of the solar collector are design variables, objective function, constraints, and optimization algorithms. These components are defined as follows:

1- Design variables

The design variables are the geometrical dimensions of the solar air collector by its width (W) the length (L), the number of channels (N), and twisted tape ratio (Y) of the solar collector.

2- Objective function

The two main objectives to be maximized are the heat gain and thermal efficiency as well as one objective to be minimized is pressure drop.

3- Constraints

The constraints of the design variables are based on the minimum and maximum levels of each design variable. For geometrical quantities, this is given as follows:

$$\begin{aligned}
 \underline{L}_{min} &\leq L \leq \overline{L}_{max} \\
 \underline{W}_{min} &\leq W \leq \overline{W}_{max} \\
 \underline{N}_{min} &\leq N \leq \overline{N}_{max} \\
 \underline{Y}_{min} &\leq Y \leq \overline{Y}_{max}
 \end{aligned}
 \tag{29}$$

Where  $L_{min}$  and  $L_{max}$  are the minimum and maximum values of collector’s length respectively.  $W_{min}$  and  $W_{max}$  are the minimum and maximum values of the collector’s width respectively.  $N_{min}$  and  $N_{max}$  are the minimum and maximum values for the number of channels respectively.  $Y_{min}$  and  $Y_{max}$  are the minimum and maximum values for

the twisted tape ratio respectively. All boundary values are defined to cover the most common values used in solar air heater collectors.

**OPTIMIZATION ALGORITHM**

The multi-objective function optimization algorithm is used to find the optimal design variables based on maximizing or minimizing the vector of the objective function. In this paper, the genetic algorithm is used to find the optimal design variables based on the objective’s functions.

Genetic algorithms are used to find the optimal solutions the minimize or maximize the objective functions. Genetic algorithms are designed based on the biological process. Therefore, much of the processes are based on genetics and natural selection. Following is the description of the genetic algorithm process [43]:

- 1- Selection of the parameters: the genetic algorithm begins to define the design variable (P) to be optimized as a chromosome. The chromosome has several parameters ( $N_{par}$ ) can be fined as

$$\begin{aligned}
 F_T(chromosome) &= F_1(P_1, P_2, P_3, \dots, P_{Npar}), \\
 &F_2(P_1, P_2, P_3, \dots, P_{Npar})
 \end{aligned}
 \tag{30}$$

- 2- Encoding and decoding: since each design variable represents a binary, genetic algorithm using the encoding and decoding process. The encoding process is to convert the continuous values into binary. Decoding is to convert the binary into continuous values. If the parameter is continuous, then it has to be quantized.

For encoding:

$$P_{norm} = \frac{P_n - P_{lo}}{P_{hi} - P_{lo}}$$

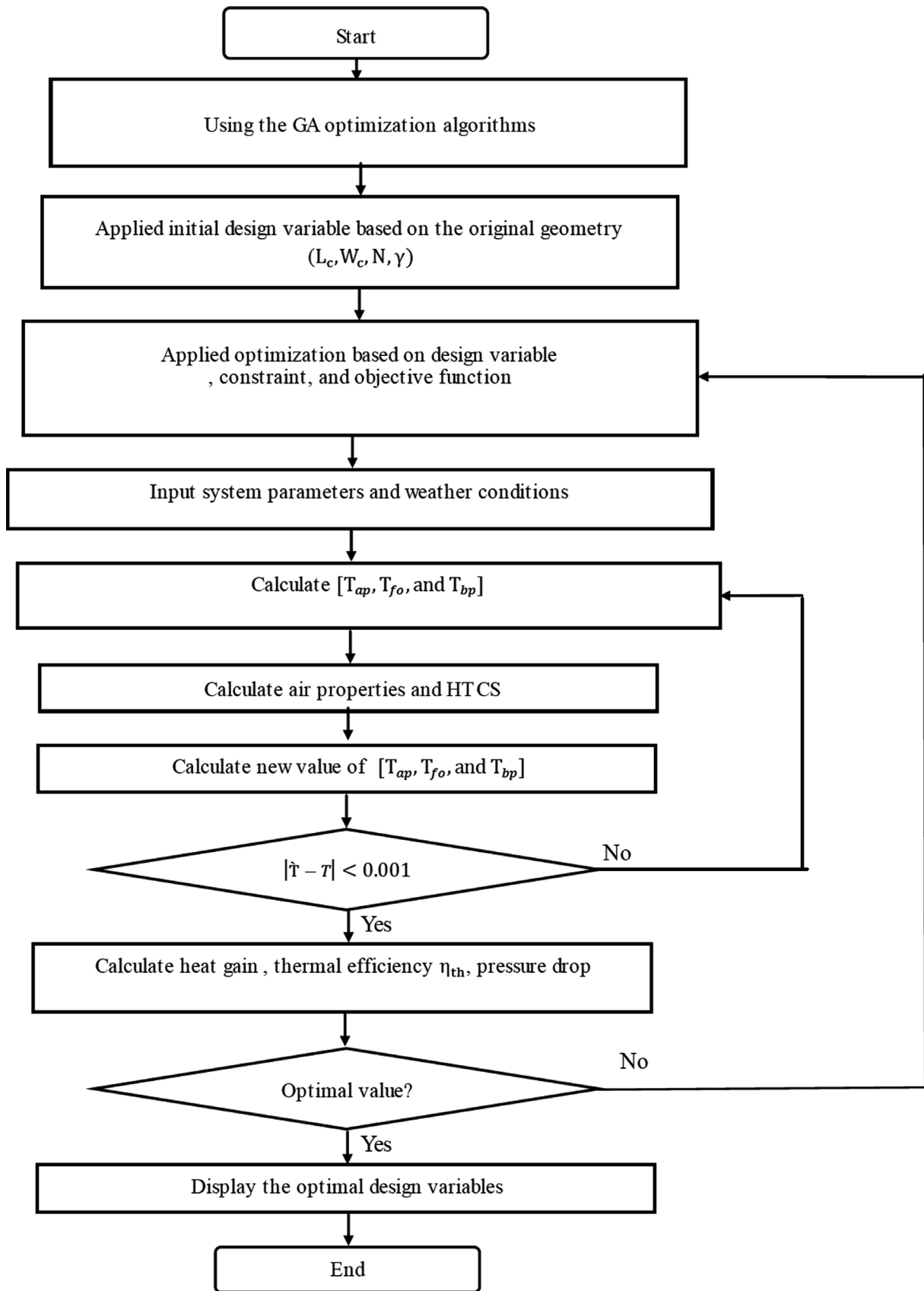


Figure 4. Flow chart for the optimization procedure of VSAH-TTI.

$$gene[m] = round\{P_{norm} - 2^{-m} - \sum_{p=1}^{m-1} gene[p]2^{-p}\} \quad (31)$$

For decoding:

$$P_{quant} \sum_{m=1}^{N_{gene}} gene[m]2^{-m} + 2^{-(M+1)} \quad (32)$$

$$q_n = P_{quan} P_{hi} - P_{lo} + P_{lo} \quad (33)$$

Where  $P_{norm}$  is normalized variable ( $0 \leq P_{norm} \leq 1$ ),  $P_{lo}$  is the smallest variable value,  $P_{hi}$  highest variable value,  $gene[m]$  binary version of  $P_n$ ,  $round\{.\}$  is round to nearest integer,  $P_{quant}$  is a quantized version of  $P_{norm}$ ,  $q_n$  is the quantized version of  $P_n$ .

- 3- The Population: is a group of chromosomes  $N_{pop}$  filled the matrix  $N_{pop} \times N_{bits}$  with random ones and zero

$$pop = round(rand(N_{pop}, N_{bits})) \quad (34)$$

- 4- Natural Selection: in this process choosing the chromosomes with the highest cost. then the only best chromosomes are selected to continue.

$$N_{keep} = X_{rate} N_{pop} \quad (35)$$

**Table 3.** Geometry and operating parameters of the mathematical model.

Parameter	Symbol	Value/Range
<b>Geometry parameters</b>		
Absorptivity of heated surface	$\alpha_p$	0.96
Emittance of heated surface	$e_p$	0.95
Emittance of backplate	$e_b$	0.95
Emittance of cover	$e_c$	0.9
Length of collector	$L$	1-2.5 m
Twist ratio	$Y$	1
Stefan-Boltzmann constant	$s$	$5.67 \times 10^{-8} \text{ Wm}^{-2} \text{ K}^{-4}$
Thickness of back insulation	$d_i$	0.05 m
Holz100 Thermal walls conductivity	$l_i$	$0.079 \text{ Wm}^{-1} \text{ K}^{-1}$
Transmittance of a glass cover	$t_c$	0.88
Width of collector	$W$	0.5-1.5 m
Number of air passages	$N$	4-14
<b>Operating parameters</b>		
Reynolds number	$Re$	1000-20000
Solar irradiance	$G$	1000 $\text{W/m}^2$
Ambient temperature	$T_{amb}$	27°C
Inlet air temperature	$T_{fi}$	30°C
Velocity of wind	$V_w$	2.5 $\text{m s}^{-1}$
Energy conversion factor	$C_f$	0.18

- 5- Pairing: two chromosomes are selected to produce two new offspring. Pairing accrue in the mating population until the  $(N_{pop} - N_{keep})$  offspring replace the discarded chromosomes
- 6- Mating: after selecting the parents in the pairing process, Mating create one or more offspring
- 7- Mutations: in this process, the genetic algorithm specifies the cost surface from  $N_{pop} \times N_{keep}$  the section in the population matrix.

The genetic algorithm is iterated until the chromosome gives the same value of cost. this means the genetic algorithm has been converged

### FLOW CHART OF THE OPTIMIZATION PROCEDURE

This section presents the optimization procedure to find the optimal dimensions of VSAH-TTI. As shown in figure 4, choosing the genetic optimization algorithm is the first step in this procedure to find the optimal dimensions of VSAH-TTI. Specify the initial value of the design variables based on the original geometry of VSAH-TTI. In this paper, the design variables are length of collector  $L_c$ , width of the collector  $W_c$ , number of channels  $N$ , and twisted tape ratio. The objective functions used on the genetic optimization algorithm to be maximized are the heat gain, thermal and effective efficiency and to be minimized is the pressure drop on solar collector. Calculation the thermal performance of the VSAH-TTI based on the energy equations to specify the objective functions of the optimization procedure. Genetic optimization algorithm is running until find the optimal dimensions of VSAH-TTI based on the objective functions.

### V-CORRUGATED ABSORBER SOLAR AIR HEATER INTEGRATED WITH TWISTED TAPE INSERTS UNDER STUDY

The geometrical parameters and the operating parameters of V-corrugated absorber solar air heater integrated with twisted tape inserts are shown in table 1. This table shows the original geometry of solar collector under study.

### THE THERMAL PERFORMANCE OF SOLAR AIR HEATER IN DIFFERENT DESIGN VARIABLES

This section shows the effect of changing the design variables on the thermal performance of VSAH-TTI model. The geometrical parameters of VSAH-TTI are length, width, twisted tape ratio, and channel number VSAH. Before applying the optimization algorithm, the thermal performance of each design variable is studied to clarify the influence of these dimensions on the VSAH-TTI.

Figure 5 shows the effect of different lengths of VSAH-TTI in the distribution of the heat gain and the thermal efficiency based on increasing the Reynolds number from

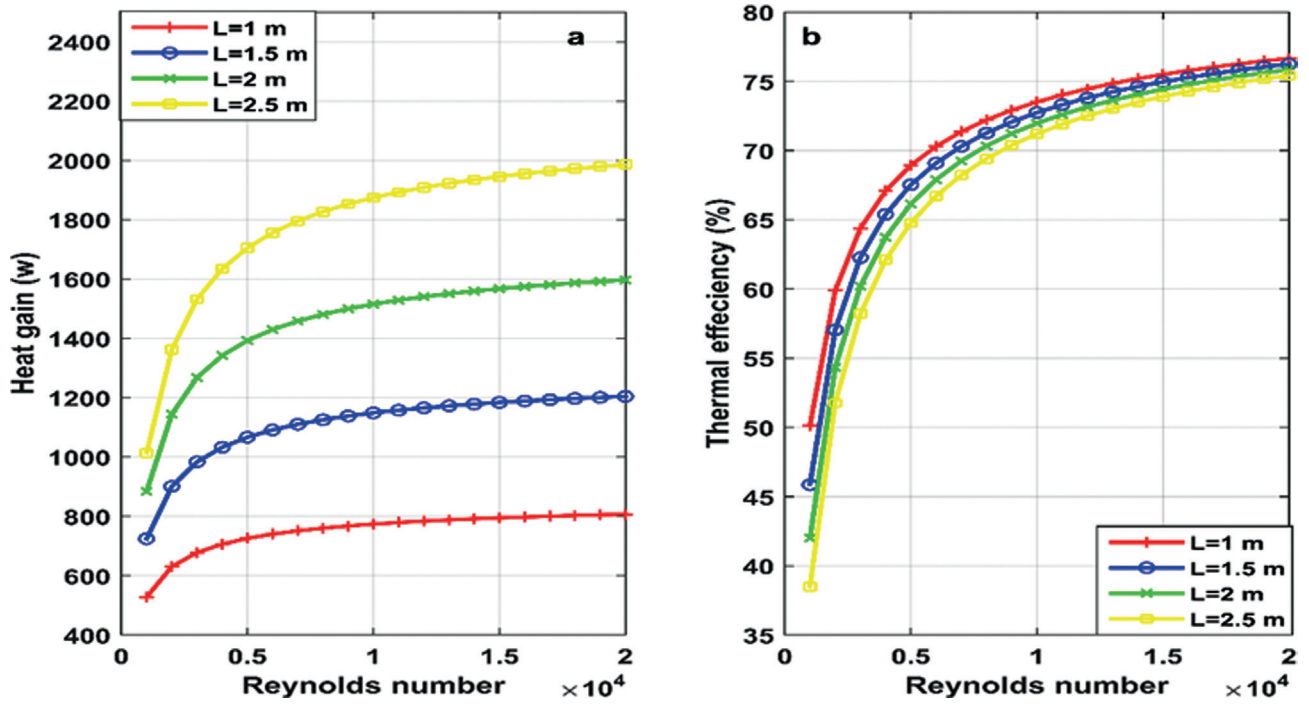


Figure 5. Effect of collector length on the (a) heat gain, and (b) thermal efficiency.

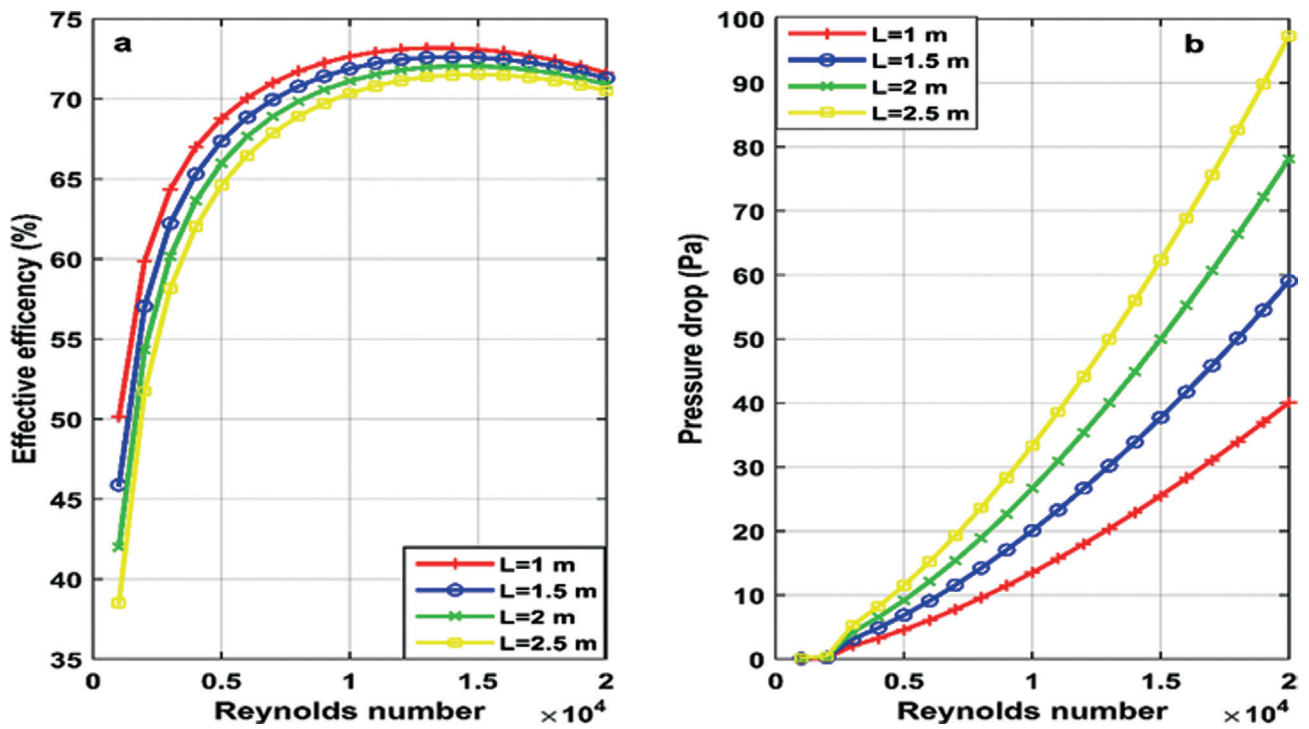


Figure 6. Effect of collector length on the (a) effective efficiency, and (b) pressure drop.

1000 to 20,000 in step 1000. This figure reveals that heat gain increases with an increase in the length of VSAH-TTI for all values of  $Re$ . It can be attributed to two reasons, first when  $Re$  increasing, the convective heat transfer coefficient increasing. Second, when collector length increases which means more time for heat transfer rate between the absorbing plate and the flowing air. However, the thermal efficiency increases when increasing the Reynolds number and decreases as the length of the collector increases due to the increase of the projected area of VSAH-TTI and increasing the top heat loss.

The effect of different collector's length on the effective efficiency and pressure drop for different values of  $Re$  is shown in figure 6(a). It can be noted that as the  $Re$  increases, the effective efficiency first increases to a specified range of  $Re$ , arrives at the maximum value, after that it falls due to pressure loss coupled with a higher  $Re$ . When  $Re > 13,000$ , the increase in the heat transfer rate was less than the rise in the pressure drop inside the collector thereby, the effective efficiency reduces dramatically at  $Re > 15,000$ . Figure 6(b) shows that the pressure drops across the collector augment progressively with rising both of collector length and  $Re$ . It is attributed to the increase in the friction losses between airflow and collector channel walls.

Figures 7(a & b) illustrates the effect of changing the width of VSAH-TTI on heat gain and thermal efficiency in different ranges of Reynolds numbers. For a specific value

of collector width, it is revealing that heat gain and thermal efficiency are directly proportional with  $Re$ . Also, it is clear from figures 7(a & b) that when the collector width increases, the heat gain increases due to the increase in the width of the air passage whereas the thermal efficiency decreases due to the increase of the projected area of the collector.

Figure 8(a & b) displays the impact of the collector width on effective efficiency and pressure for different values of  $Re$ , respectively. Figure 8(a) indicated that, as the collector width increases, effective efficiency is increased to a certain value of Reynolds number, getting the highest value, and then falls due to a high level of pressure loss.

It can be noted that the cross-sectional area of the flow duct at  $W = 0.5$  is less than that for other values of  $W$ . Thereby, a greater pressure drop has been recorded at  $W$  of 0.5 than that the rest  $W$  values, and less energy carried out by the working fluid due to high air velocity inside the flow duct for the  $W = 0.5$  than that for the other  $W$  values. As a result, the behaviour of the effective efficiency will drop firstly at  $W = 0.5$  than that the rest  $W$  values. On the other hand, as shown in Figure 8(b), the pressure drop is decreased with increases in the width of the collector. It is attributed to the large cross-sectional area of the flow channel which means low velocity inside each channel, thereby low friction losses occur between the air and the channel walls.

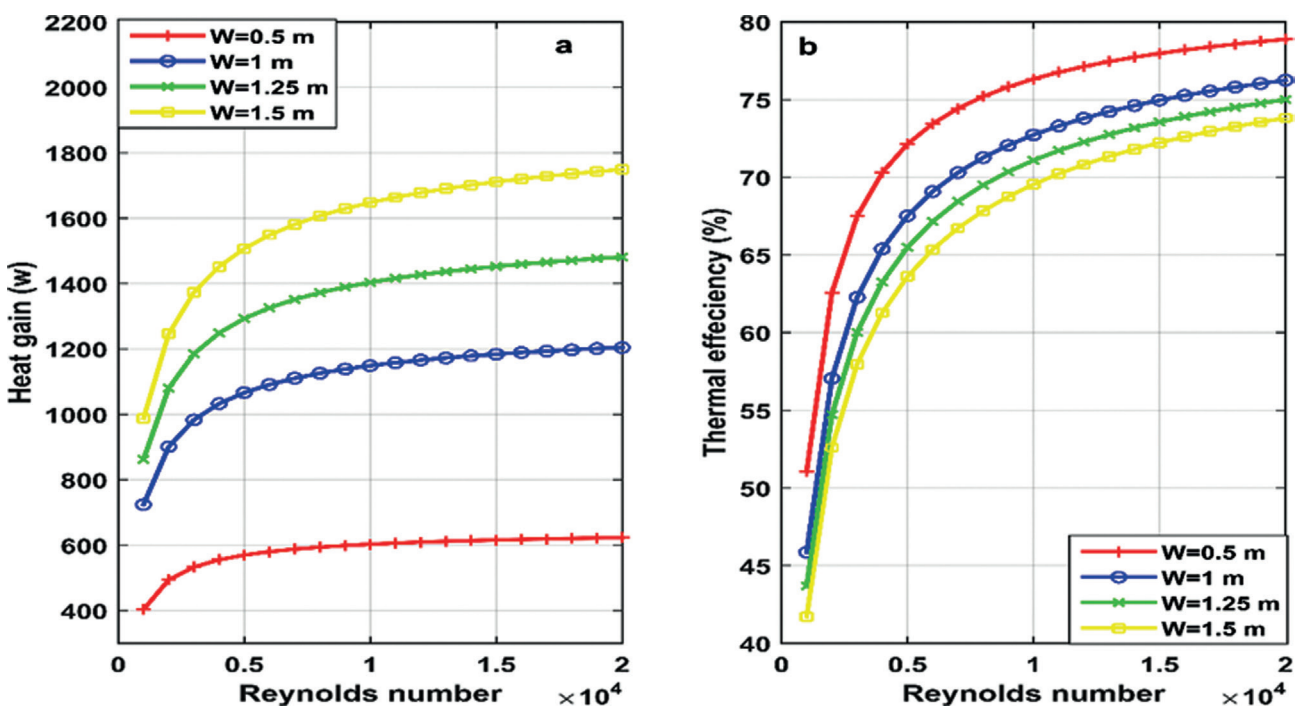


Figure 7. Effect of collector width on the (a) heat gain, and (b) thermal efficiency.

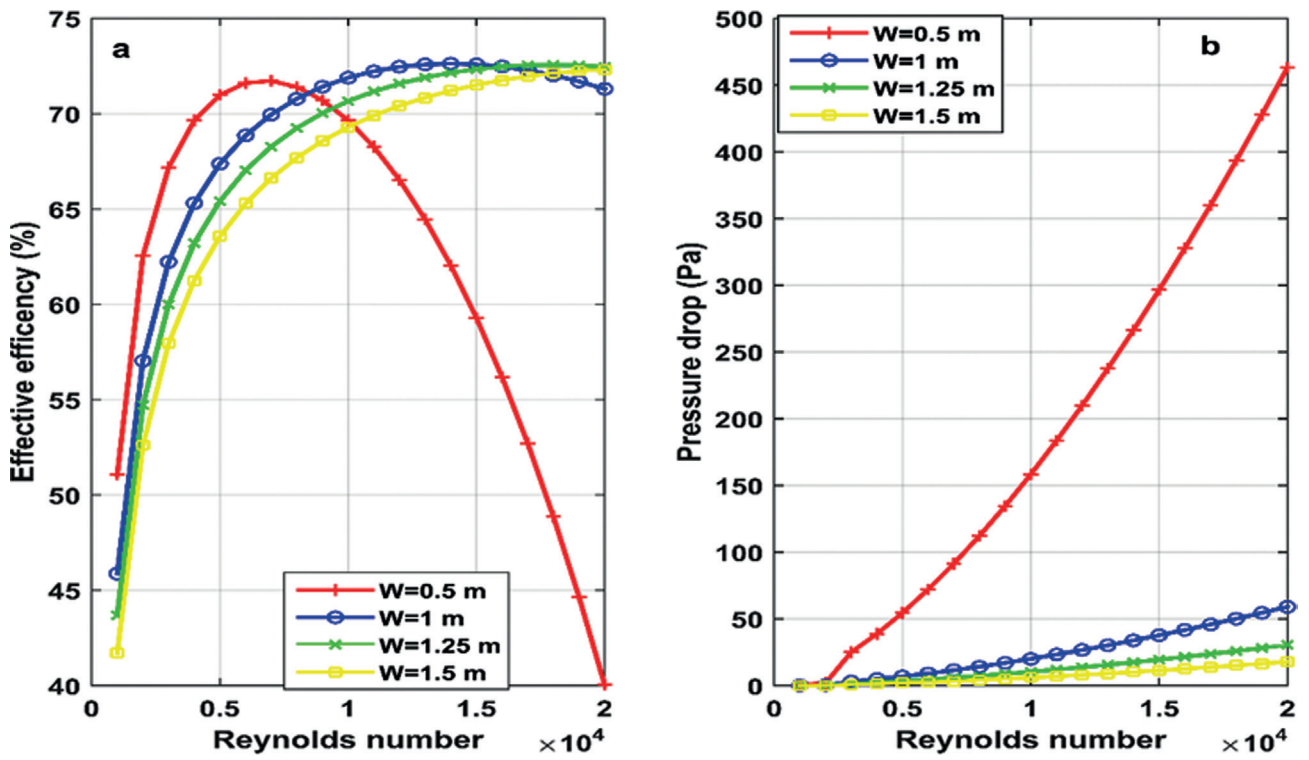


Figure 8. Effect of collector width on the (a) effective efficiency, and (b) pressure drop.

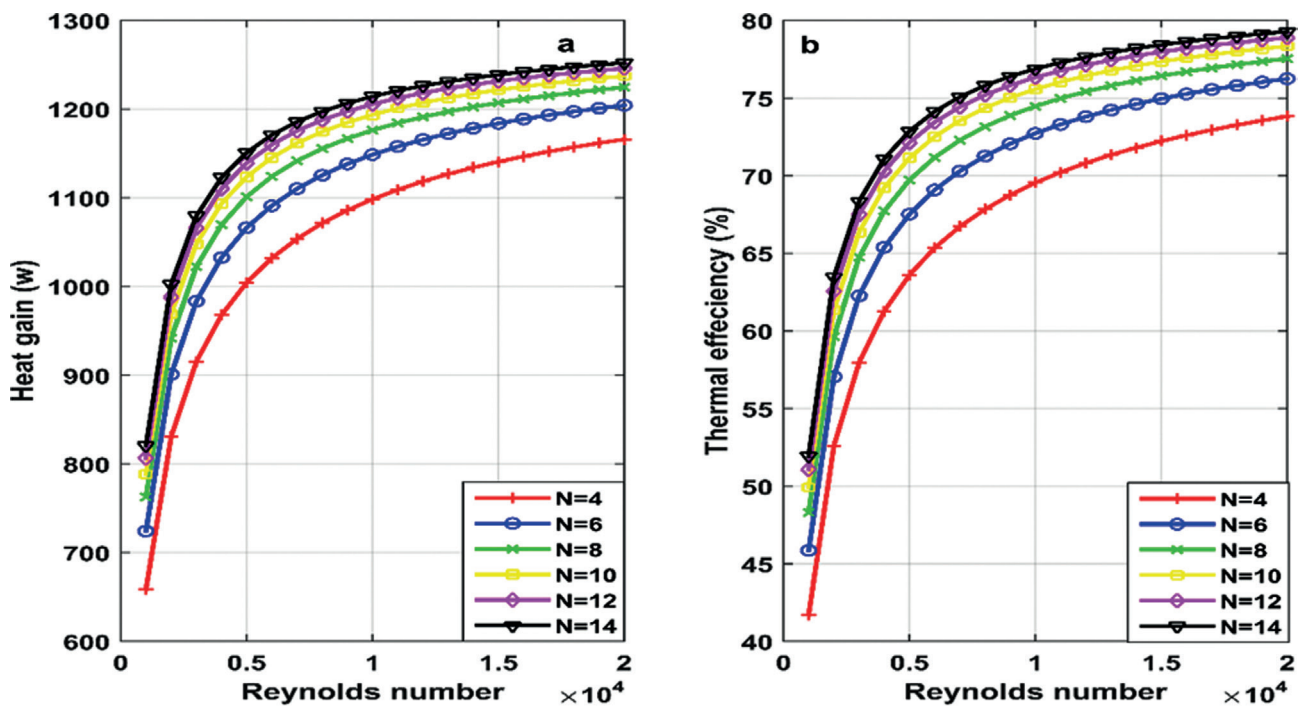


Figure 9. Effect of channel numbers on the (a) heat gain, and (b) thermal efficiency.

Figure 9 depicts the effect of  $N$  on heat gain and thermal efficiency for VSAH-TTI for various ranges of  $Re$ . From figure 9(a & b), it can be noted with increases of  $N$  values, both the heat gain and thermal efficiency grow up exponentially till  $Re > 10,000$ . After that, a linear relation between heat gain and thermal efficiency with  $N$  is found due to increment in the  $Re$  and  $N$  lead to the rise of air velocity inside flow channels and then increases the heat transfer coefficient. Also, the increment in  $N$  values leads to generate a swirl flow which produces more heat transfer rate between the absorbing plate and the airflow.

Figure 10 shows the influence of increased channel numbers on the effective efficiency and the pressure drop for the various values of  $Re$ . Figure 10(a) reveals that the effective efficiency rises with increases  $Re$  till  $Re > 6000$  which arrives at the maximum value. After that, for  $4 \leq N \leq 6$ , effective efficiency is linearly increasing. While for  $8 \leq N \leq 14$ , a remarkable collapse is occurring in the effective efficiency. It is attributed to the increases in pressure loss related to the dominant turbulent region related to increases in channel numbers. It can be reported that the  $N = 6$  award best effective efficiency comparing with all other cases.

The impact of channel numbers on the pressure loss across the solar collector is presented in Figure 10(b). It seems that the pressure drop across the collector channel raises with increases both of  $Re$  and the channel numbers. It can be noted that a small growth in the pressure loss

occurs when the  $N$  increases from 4 to 8. While pressure drop increases noticeably when  $N$  rises from 10 to 14. It is found that the pressure drops related to  $N = 14$  are greater than that for  $N = 6$  for a given  $Re$ . It is attributed to high velocity inside the channel when  $N = 14$  which leads to high friction losses and high vortices due to the presence of TTI in comparison to  $N = 6$ .

Figure 11(a & b) shows the impact of  $Y$  on heat gain and thermal efficiency for various ranges of  $Re$ . Heat gain and thermal efficiency are increased with rises of  $Re$  and  $Y$ . It is attributed to good air mixing inside the flow channel of the solar air collector due to the existence of TTI which produces vortex flow which enhances heat transfer rate.

Thermo-hydraulic efficiency is the major parameter to be considered when calculating the performance of VSAH. Thermo-hydraulic efficiency is affected by the variation of  $Y$  as shown in Figure 12(a). The results show that when  $Y$  values reduce, thermos-hydraulic performance is raised at the beginning, as  $Re$  increases, until it reaches the maximum value at a certain value of  $Re$ , after that it starts to fall as expected due to large friction loss occurs at a lower value of  $Y$ . Figure 12(b) indicates the variation in the pressure drop with various values of  $Y$ . It is noticed that pressure losses increase with decreases in  $Y$  due to reasons explained above. Moreover, at  $Y = 1$ , the maximum value of thermo-hydraulic efficiency is 73% at  $Re = 13000$  against the pressure drop of 59 Pa at  $Re = 20000$ .

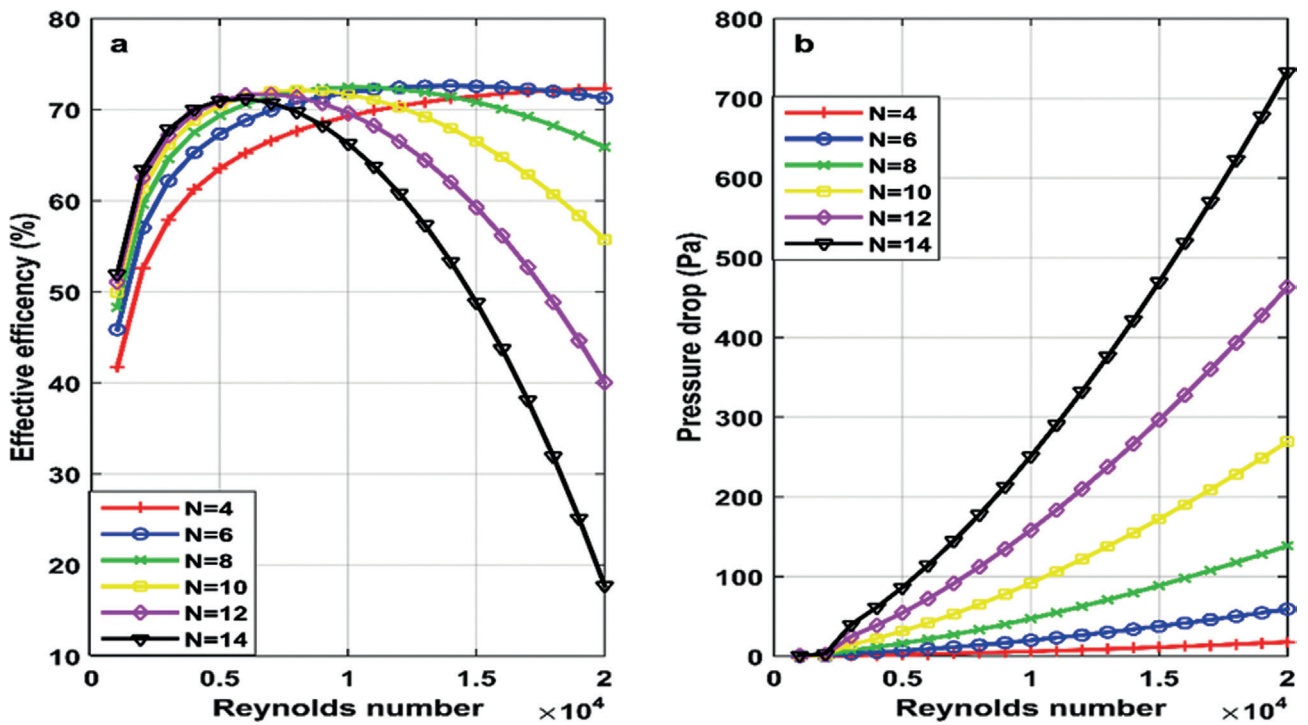


Figure 10. Effect of channel numbers on the (a) effective efficiency, and (b) pressure.

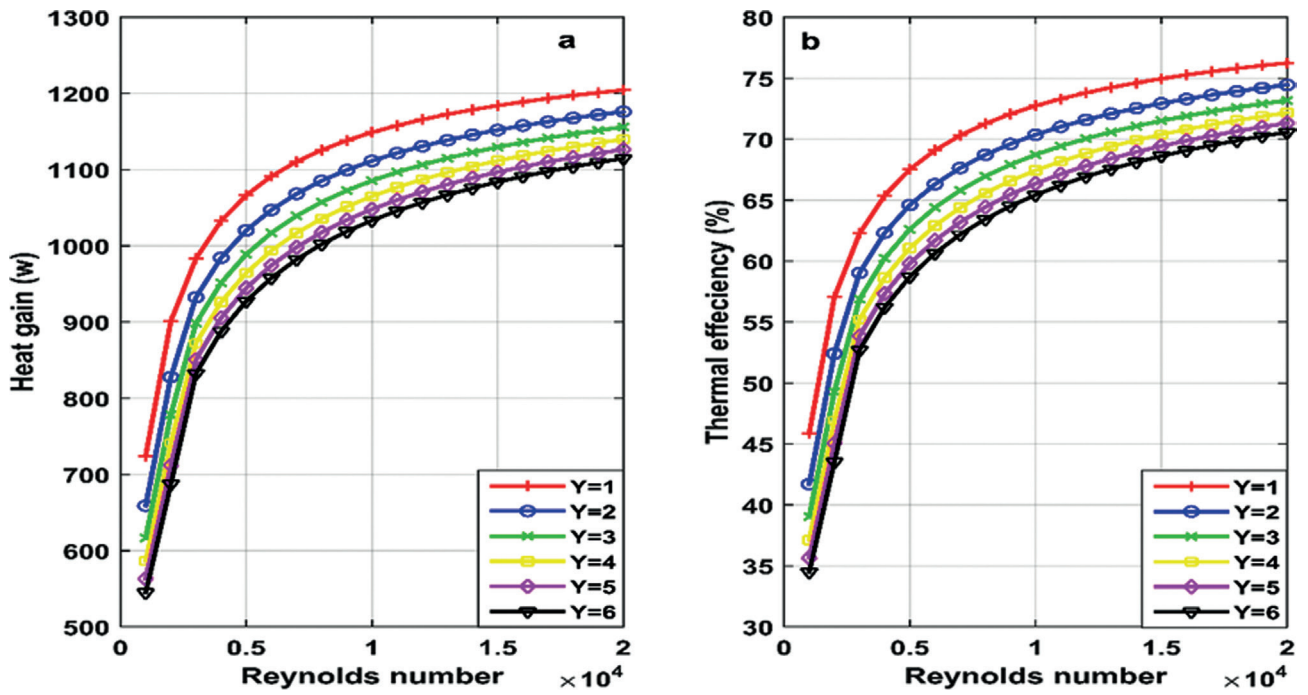


Figure 11. Influence of  $Y$  on the (a) heat gain, and (b) thermal efficiency.

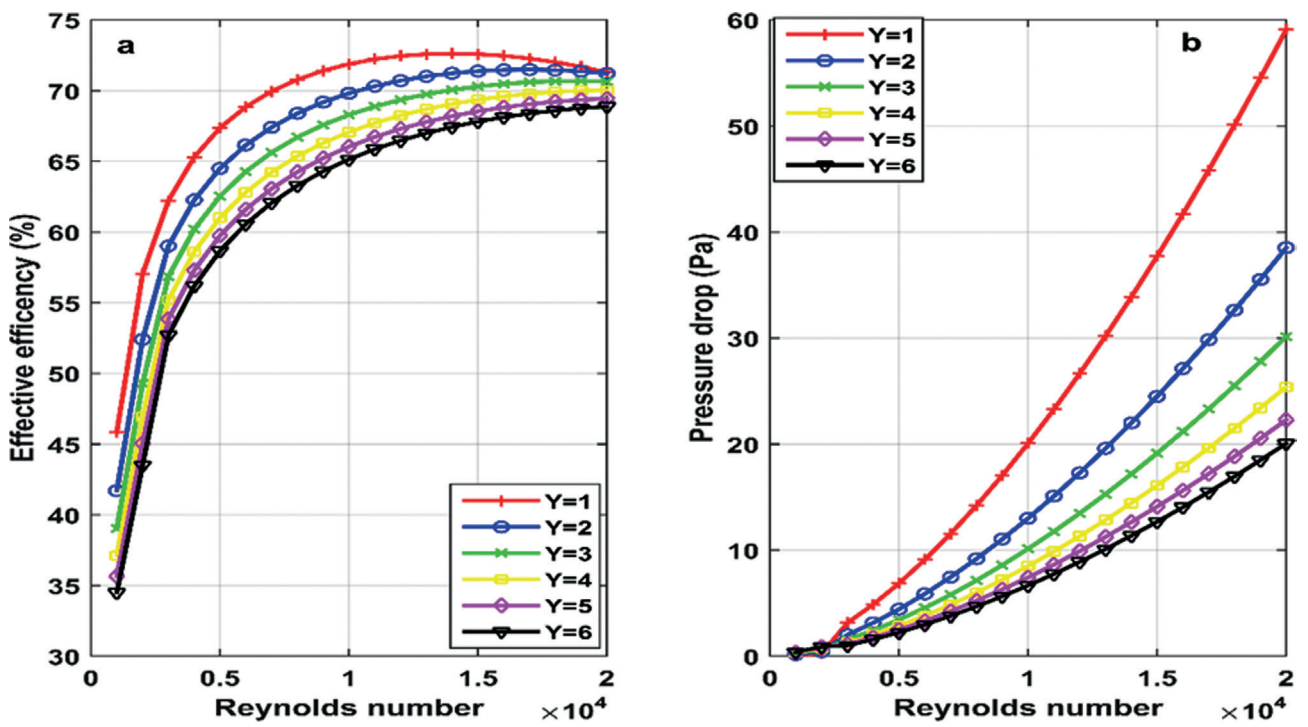


Figure 12. Influence of  $Y$  on the (a) effective efficiency, and (b) pressure drop.

**Table 4.** Constraints of design variables

Variables	Minimum	Maximum
Length of VSAH	1	2.5
Width of VSAH	0.5	1.5
Number of channels	4	14
Twisted tape ratio	1	8

**Table 5.** design variables of FDPSAH

Variables	Original	Optimized
Length of SAH	1.5	1.0195
Width of SAH	1	1.4932
Number of Channel	4	6
Twisted ration	1	1

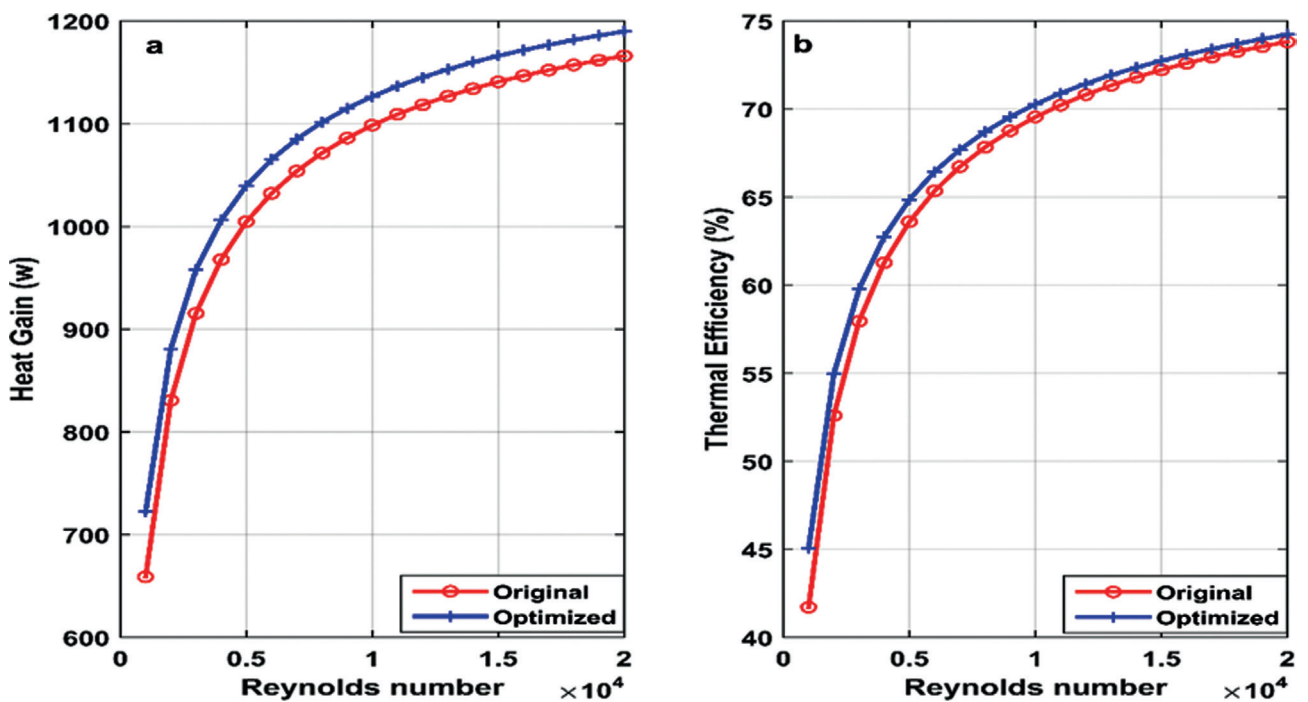


**Figure 13.** The heat gain and thermal efficiency for original and optimal design.

As shown in figures (11 and 12), the different behaviors of heat gain, thermal efficiency, effective efficiency, and pressure drop with changing the design variables of VSAH-TTI. Therefore, finding the optimal design of VSAH-TTI based on maximizing the heat gain, thermal efficiency, and effective efficiency as well as minimizing the pressure drop is extremely complicated. This paper using a multi-objective optimization genetic algorithm to find the optimal geometry aimed to maximize the heat gain, thermal efficiency, and effective efficiency as well as minimizing the pressure drop as shown in the next section.

**OPTIMAL GEOMATIC DESIGN OF VSAH-TTI**

In this paper, the multi-objective optimization algorithm by using a genetic algorithm is used to find the

optimal geometric parameters of VSAH-TTI. The objective functions of the optimization algorithms to be maximized are the heat gain, thermal efficiency, and effective efficiency, in addition, to be minimized is the pressure drop. The constrain in each design variable are most important in the optimization algorithm. In this paper, the constrain of design variables are selected based on the most common range of solar air collectors as shown in Table 4.

**OPTIMAL GEOMETRICAL PARAMETERS OF VSAH-TTI**

The multi-objective function genetic algorithm is applied to find the optimal geomatic parameters for the VSAH-TTI based on maximizing the heat gain, thermal efficiency, and effective efficiency as well as minimizing

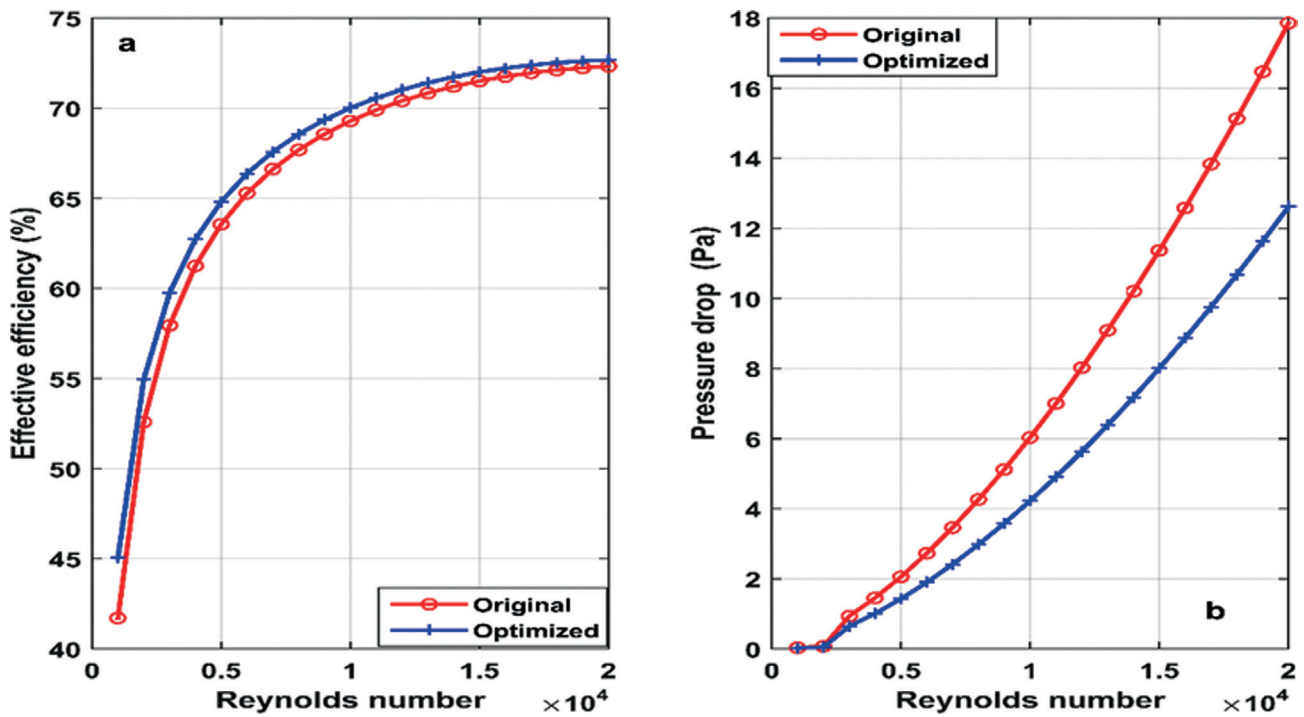


Figure 14. The effective efficiency and pressure drop for original and optimal design.

pressure drop. The constraints of each design variable are specified in Table 4. The optimal design variables after applied the multi-objective function genetic algorithm are listed in Table 5 for the VSAH-TTI as well as the original parameters for the case under study.

This section shows the comparison in thermal performance between the optimized geometric parameters by using a genetic algorithm and the original parameters. Figure 13(a & b) illustrates the heat gain and thermal efficiency against the Reynold number by using original and optimized geometry. As shown in both figures the optimized geometry by using a genetic algorithm gives higher heat gain and thermal efficiency than the original geometry.

Furthermore, the optimized geometry can provide higher effective efficiency than the original geometry as shown in figure 14(a). Also, Pressure drop in optimized geometry is less than the original geometry based on different Reynolds numbers as shown in figure 14(b).

It can be concluded from figures 13 and 14 that the optimized geometry using a genetic algorithm can enhance the thermal performance of VSAH-TTI. Based on these figures, the maximum in optimized when compare with original geometry in heat gain is 8%, thermal efficiency is 7.5%, effective efficiency is 7.5%. As well as, there was a remarkable reduction in pressure drop by about 30%.

## CONCLUSION

This paper proposed a method to find the optimal dimensions of VSAH-TTI. The mathematical model of VSAH-TTI was presented based on the energy balance technique. Multi-objective function genetic algorithm was used to find the optimal dimensions of VSAH-TTI based on maximizing the heat gain, thermal efficiency, and effective efficiency as well as minimizing pressure drop. Length of collector, the width of collector, number of channels, number of twisted tape ratio were the main design variables in the optimization algorithm. From the results, the following conclusions are obtained:

- 1- The results showed for the case under study that the heat gain, thermal efficiency, effective efficiency, and pressure drop had different behaviours when changing the geometrical parameters of VSAH-TTI in different Re.
- 2- the results showed the optimal geometry by using genetic algorithms had the highest improvement in heat gain, thermal efficiency, and effective efficiency than the original geometry. The maximum percentage improvement when an applied range of Reynold number (0-20000) was more than 8% heat gain and 7.5% of thermal and effective efficiency for the original VSAH-TTI geometry. Also, a remarkable reduction in pressure drop was achieved when

applying the same range of Reynold number by about 30% compared with the original VSAH-TTI geometry.

- 3- This proposed method showed an efficient approach to find the optimal geometrical dimensions for VSAH-TTI. Furthermore, the optimized geometry can increase the thermal efficiency and heat gain, effective efficiency as well as reducing the pressure drop without adding new materials to the VSAH-TTI.

According to our expectations, the optimal parameters reported in this research will be studied experimentally and numerically by CFD program to show the thermal distribution and fluid flow. According to the research outcomes, system efficiency may be improved as well as its application range expanded, which might include drying and space heating, among other applications.

## NOMENCLATURE

$A_p$	surface area of the heated surface (m <sup>2</sup> )
$b$	half-height of the flow passage
$C_f$	correction factor
$c_p$	specific heat of the air (J/kg K)
$D_h$	hydraulic diameter
$f$	friction factor
$h$	convective heat transfer coefficient (W/m <sup>2</sup> K)
$h_r$	coefficient of radiation heat transfer (W/m <sup>2</sup> K)
$h_w$	wind heat transfer coefficient (W/m <sup>2</sup> K)
$H$	twisted tape height (m)
$G$	solar irradiance (W/m <sup>2</sup> )
$L$	collector length (m)
$\dot{m}_f$	air mass flowrate (kg/s)
$Nu$	Nusselt number
$P$	pitch for 180° rotation of twisted tape (m)
$P_p$	pumping power consumption (W)
$Q_u$	useful heat gain (W)
$Re$	Reynolds number
$T_{amb}$	ambient temperature (K)
$T_b$	average temperature of the backplate (K)
$T_f$	air temperature (K)
$T_{fi}$	inlet air temperature (K)
$T_{fo}$	outlet air temperature (K)
$T_p$	average temperature of the absorbing plate (K)
$U_b$	bottom lose coefficient (W/m <sup>2</sup> K)
$U_t$	top loss coefficient (W/m <sup>2</sup> K)
$W$	Collector width (m)
<i>Greek letters</i>	
$\alpha_p$	absorptance of the absorber plate
$d_i$	thickness of bottom insulation (m)
$DP$	pressure drop (Pa)
$e_p$	absorbing plate emissivity

$e_b$	backplate emissivity
$r$	density of air (kg/m <sup>3</sup> )
$h_{th}$	thermal efficiency (%)
$h_{h-th}$	hydro-thermal efficiency (%)
$l$	thermal conductivity of air (W/m K)
$l_i$	thermal conductivity of bottom insulation (W/m K)
$m$	dynamic viscosity of air (Pa s)
$s$	Stefan–Boltzmann constant (W/m <sup>2</sup> K <sup>4</sup> )
$t_c$	transmittance of the glazing cover
<i>Subscript</i>	
$b-f$	Bottom plate to airflow
$p-b$	Absorbing plate to bottom plate
$p-f$	Absorbing plate to airflow

## AUTHORSHIP CONTRIBUTIONS

Authors equally contributed to this work.

## DATA AVAILABILITY STATEMENT

The authors confirm that the data that supports the findings of this study are available within the article. Raw data that support the finding of this study are available from the corresponding author, upon reasonable request.

## CONFLICT OF INTEREST

The author declared no potential conflicts of interest with respect to the research, authorship, and/or publication of this article.

## ETHICS

There are no ethical issues with the publication of this manuscript.

## REFERENCES

- [1] Gao W, Lin W, Liu T, Xia C. Analytical and experimental studies on the thermal performance of cross-corrugated and flat-plate solar air heaters. *Appl Energy* 2007;84:425–441. [\[CrossRef\]](#)
- [2] Upadhyay BH, Patel AJ, Sadasivuni KK, Mistry JM, Ramana PV, Panchal H, et al. Design, development and techno economic analysis of novel parabolic trough collector for low-temperature water heating applications. *Case Stud Therm Eng* 2021;26:100978. [\[CrossRef\]](#)
- [3] Panchal H, Mevada D, Sadasivuni KK, Essa FA, Shanmugan S, Khalid M. Experimental and water quality analysis of solar stills with vertical and inclined fins. *Groundw Sustain Dev* 2020;11:100410. [\[CrossRef\]](#)

- [4] Mevada D, Panchal H, Kumar Sadasivuni K, Israr M, Suresh M, Dharaskar S, et al. Effect of fin configuration parameters on performance of solar still: A review. *Groundw Sustain Dev* 2020;10:100289. [\[CrossRef\]](#)
- [5] Panchal H, Sathyamurthy R. Experimental analysis of single-basin solar still with porous fins. *Int J Ambient Energy* 2020;41:563–569. [\[CrossRef\]](#)
- [6] Natarajan K, Thokchom SS, Verma TN, Nashine P. Convective solar drying of *Vitis vinifera* & *Momordica charantia* using thermal storage materials. *Renew Energy* 2017;113:1193–1200. [\[CrossRef\]](#)
- [7] Fudholi A, Sopian K, Ruslan MH, Othman MY, Yahya M. Analytical and experimental studies on the thermal efficiency of the double-pass solar air collector with finned absorber. *Am J Appl Sci* 2011;8:716–723. [\[CrossRef\]](#)
- [8] Hans VS, Saini RP, Saini JS. Heat transfer and friction factor correlations for a solar air heater duct roughened artificially with multiple v-ribs. *Sol Energy* 2010;84:898–911. [\[CrossRef\]](#)
- [9] Farhan AA, Sahi HA. Energy analysis of solar collector with perforated absorber plate. *J Eng* 2017;23:289–102.
- [10] Yang M, Yang X, Li X, Wang Z, Wang P. Design and optimization of a solar air heater with offset strip fin absorber plate. *Appl Energy* 2014;113:1349–1362. [\[CrossRef\]](#)
- [11] Jain SK, Agrawal GD, Misra R. A detailed review on various V-shaped ribs roughened solar air heater. *Heat Mass Transf* 2019;55:3369–3412. [\[CrossRef\]](#)
- [12] Sivakandhan C, Arjunan TV, Matheswaran MM. Thermohydraulic performance enhancement of a new hybrid duct solar air heater with inclined rib roughness. *Renew Energy* 2020;147:2345–2357. [\[CrossRef\]](#)
- [13] Bhagoria JL, Saini JS, Solanki SC. Heat transfer coefficient and friction factor correlations for rectangular solar air heater duct having transverse wedge shaped rib roughness on the absorber plate. *Renew Energy* 2002;25:341–369. [\[CrossRef\]](#)
- [14] Singh I, Singh S. CFD analysis of solar air heater duct having square wave profiled transverse ribs as roughness elements. *Sol Energy* 2018;162:442–453. [\[CrossRef\]](#)
- [15] Priyam A, Chand P. Effect of wavelength and amplitude on the performance of wavy finned absorber solar air heater. *Renew Energy* 2018;119:690–702. [\[CrossRef\]](#)
- [16] Skullong S, Promvong P, Thianpong C, Pimsarn M. Thermal performance in solar air heater channel with combined wavy-groove and perforated-delta wing vortex generators. *Appl Therm Eng* 2016;100:611–620. [\[CrossRef\]](#)
- [17] Kumar R, Goel V, Kumar A. Investigation of heat transfer augmentation and friction factor in triangular duct solar air heater due to forward facing chamfered rectangular ribs: A CFD based analysis. *Renew Energy* 2017;115:824–835. [\[CrossRef\]](#)
- [18] Ghrilahre HK, Sahu PK, Chand S. Thermal performance and heat transfer analysis of arc shaped roughened solar air heater – An experimental study. *Sol Energy* 2020;199:173–182. [\[CrossRef\]](#)
- [19] Saini RP, Varun, Singal SK. A review on roughness geometry used in solar air heaters. *Sol Energy* 2007;81:1340–1350. [\[CrossRef\]](#)
- [20] Mahanand Y, Senapati JR. Thermo-hydraulic performance analysis of a solar air heater (SAH) with quarter-circular ribs on the absorber plate: A comparative study. *Int J Therm Sci* 2021;161:106747. [\[CrossRef\]](#)
- [21] Gupta MK, Kaushik SC. Exergetic performance evaluation and parametric studies of solar air heater. *Energy* 2008;33:1691–1702. [\[CrossRef\]](#)
- [22] Nwosu NP. Employing exergy-optimized pin fins in the design of an absorber in a solar air heater. *Appl Sol Energy* 2009;45:248–253. [\[CrossRef\]](#)
- [23] Layek A. Optimal thermo-hydraulic performance of solar air heater having chamfered rib-groove roughness on absorber plate. *Int J Energy Environ* 2010;1:683–696. [\[CrossRef\]](#)
- [24] Siddhartha, Sharma N, Varun. A particle swarm optimization algorithm for optimization of thermal performance of a smooth flat plate solar air heater. *Energy* 2012;38:406–413. [\[CrossRef\]](#)
- [25] Sahin AS. Optimization of solar air collector using genetic algorithm and artificial bee colony algorithm. *Heat Mass Transf* 2012;48:1921–1928. [\[CrossRef\]](#)
- [26] Kumar A, Kim MH. Numerical optimization of solar air heaters having different types of roughness shapes on the heated plate - Technical note. *Energy* 2014;72:731–738. [\[CrossRef\]](#)
- [27] Prasad BN, Kumar A, Singh KDP. Optimization of thermo hydraulic performance in three sides artificially roughened solar air heaters. *Sol Energy* 2015;111:313–319. [\[CrossRef\]](#)
- [28] Kulkarni K, Afzal A, Kim KY. Multi-objective optimization of solar air heater with obstacles on absorber plate. *Sol Energy* 2015;114:364–377. [\[CrossRef\]](#)
- [29] Venkata Rao R, Waghmare G. Optimization of thermal performance of a smooth flat-plate solar air heater using teaching-learning-based optimization algorithm. *Cogent Eng* 2015;2:997421. [\[CrossRef\]](#)
- [30] Zhuang C, Fu B, Huang G, Zhang H. Optimization of the structure of a solar air heater fitted with v-shaped perforated baffles. *Int J Heat Technol* 2016;34:604–610. [\[CrossRef\]](#)
- [31] Acir A, Canlı ME, Ata I, Cakıroğlu R. Parametric optimization of energy and exergy analyses of a

- novel solar air heater with grey relational analysis. *Appl Therm Eng* 2017;122:330–338. [\[CrossRef\]](#)
- [32] Nadda R, Kumar R, Kumar A, Maithani R. Optimization of single arc protrusion ribs parameters in solar air heater with impinging air jets based upon PSI approach. *Therm Sci Eng Prog* 2018;7:146–154. [\[CrossRef\]](#)
- [33] Ansari M, Bazargan M. Optimization of flat plate solar air heaters with ribbed surfaces. *Appl Therm Eng* 2018;136:356–363. [\[CrossRef\]](#)
- [34] Kumar R, Goel V, Singh P, Saxena A, Kashyap AS, Rai A. Performance evaluation and optimization of solar assisted air heater with discrete multiple arc shaped ribs. *J Energy Storage* 2019;26:100978. [\[CrossRef\]](#)
- [35] Yildirim C, Tümen Özdil NF. Theoretical investigation of a solar air heater roughened by ribs and grooves. *J Therm Eng* 2018;4:1702–1712. [\[CrossRef\]](#)
- [36] Qader BS, Supeni EE, Ariffin MKA, Talib AA. RSM approach for modeling and optimization of designing parameters for inclined fins of solar air heater. *Renew Energy* 2019;136:48–68. [\[CrossRef\]](#)
- [37] Bezbaruah PJ, Das RS, Sarkar BK. Overall performance analysis and GRA optimization of solar air heater with truncated half conical vortex generators. *Sol Energy* 2020;196:637–652. [\[CrossRef\]](#)
- [38] Farhan AA, Ali AIM, Ahmed HE. Energetic and exergetic efficiency analysis of a V-corrugated solar air heater integrated with twisted tape inserts. *Renew Energy* 2021;169:1373–1385. [\[CrossRef\]](#)
- [39] Duffie JA, Beckman WA, Blair N. *Solar Engineering of Thermal Processes, Photovoltaics and Wind*. 5th ed. New Jersey: JohnWiley& Sons; 2020.
- [40] Hollands KGT, Shewen EC. Optimization of flow passage geometry for air-heating, plate-type solar collectors. *J Sol Energy Eng* 1981;103:323–330. [\[CrossRef\]](#)
- [41] Hong SW, Bergles AE. Augmentation of laminar flow heat transfer in tubes by means of twisted-tape inserts. *J Heat Transf* 1976;98:251–256. [\[CrossRef\]](#)
- [42] Bas H, Ozceyhan V. Heat transfer enhancement in a tube with twisted tape inserts placed separately from the tube wall. *Exp Therm Fluid Sci* 2012;41:51–58. [\[CrossRef\]](#)
- [43] Prakash C, Saini RP. Heat transfer and friction in rectangular solar air heater duct having spherical and inclined rib protrusions as roughness on absorber plate. *Exp Heat Transf* 2019;32:469–487. [\[CrossRef\]](#)
- [44] Cortés A, Piacentini R. Improvement of the efficiency of a bare solar collector by means of turbulence promoters. *Appl Energy* 1990;36:253–261. [\[CrossRef\]](#)
- [45] Kumar R, Chand P. Performance prediction of extended surface absorber solar air collector with twisted tape inserts. *Sol Energy* 2018;169:40–48. [\[CrossRef\]](#)
- [46] Hedayatizadeh M, Ajabshirchi Y, Sarhaddi F, Farahat S, Safavinejad A, Chaji H. Analysis of exergy and parametric study of a V-corrugated solar air heater. *Heat Mass Transf* 2012;48:1089–1101. [\[CrossRef\]](#)
- [47] Kabeel AE, Khalil A, Shalaby SM, Zayed ME. Experimental investigation of thermal performance of flat and V-corrugated plate solar air heaters with and without PCM as thermal energy storage. *Energy Convers Manag* 2016;113:264–272. [\[CrossRef\]](#)
- [48] Jarimi H, Bakar MNA, Othman M, Din MH. Bi-fluid photovoltaic/thermal (PV/T) solar collector: Experimental validation of a 2-D theoretical model. *Renew Energy* 2016;85:1052–1067. [\[CrossRef\]](#)